



## Full length article

## Shake table tests on a full-scale six-storey cold-formed thin-walled steel-steel plate shear wall structure

Xuhong Zhou <sup>a,b</sup>, Xinmei Yao <sup>c</sup>, Lei Xu <sup>a,d</sup>, Yu Shi <sup>a,b,\*</sup>, Ke Ke <sup>a,b</sup>, Liping Liu <sup>a,b</sup>

<sup>a</sup> College of Civil Engineering, Chongqing University, Chongqing 400045, China

<sup>b</sup> Key Laboratory of New Technology for Construction of Cities in Mountain Area (Ministry of Education), Chongqing University, Chongqing 400045, China

<sup>c</sup> College of Civil Engineering, Chang'an University, Xi'an, Shaanxi, 710061, China

<sup>d</sup> Department of Civil and Environmental Engineering, University of Waterloo, Waterloo, Ontario, N2L3G1, Canada



## ARTICLE INFO

**Keywords:**

Cold-formed steel

Multi-storey

Steel plate shear wall

Shake table test

Seismic performance

## ABSTRACT

To evaluate the seismic response of a multi-storey cold-formed thin-walled steel (CFS) structure based on the influence of nonstructural members, shake table tests were conducted on a full-scale six-storey CFS-steel plate shear wall structure (SPSWS) using bidirectional seismic inputs. The building specimen was tested at two different stages. In the first stage, the specimen mainly included structural components of walls, floors, and roofs, whereas the second stage model included all the nonstructural components. The testing program and obtained results including the observed damage, dynamic characteristics, strain response, acceleration, and displacement response were presented. Overall, this study revealed that the skin effect of lightweight wall panels, together with steel plate shear walls, resisted horizontal earthquakes and demonstrated the excellent deformation capacity and seismic performance of the CFS-SPSWS building.

## 1. Introduction

CFS structures have been applied in high seismic activity regions owing to their characteristics of short construction period, high extent of assembly, excellent seismic performance, environmental protection, and energy saving. CFS structures are commonly used in low-rise residential buildings, schools, and hospitals and their use is gradually expanding to multi-storey buildings. This study focuses on the seismic response of multi-storey CFS structure buildings.

In recent years, most studies on the seismic performance of the overall CFS structure have mainly been focused on low-rise buildings. For instance, the seminal work of Peterman et al. [1,2] provided the detailed loading process and results of shake table tests on full-scale two-storey CFS oriented strand board (OSB) — sheathed structure buildings, and the influences of structural and nonstructural members on the structural dynamic characteristics and displacement response were examined. The shake table test conducted by Li et al. [3] on three full-scale two-storey high-strength CFS buildings represents the first experimental study to investigate the system-level seismic performance of CFS buildings. The horizontal lateral CFS walls were sheathed with either OSBs or corrugated sheets in the exterior walls and gypsum boards in the interior walls. The results indicated that the CFS structure buildings with composite walls constructed using these two types of double-sided sheathing plates are safe and reliable under high-intensity earthquakes. Later, Huang et al. [4] performed shake table tests on

a full-scale three-storey CFS structure, and OSB-sheathed walls were installed in the structure to resist lateral forces. The main objective of their research was to evaluate the seismic performance of low-rise CFS structure buildings. The experimental results revealed that the lateral force resistance of this building system depends on the skin diaphragm effect of OSBs and the overturning capability of hold-downs. To evaluate the influence of finishing materials on the seismic performance of CFS buildings, horizontal shake table tests were conducted by Fiorino et al. [5] on a full-scale two-storey prefabricated CFS structure building, where the walls were sheathed with gypsum board panels on both sides. Shake table tests were conducted on two reduced-scale three-storey CFS structures by Terracciano et al. [6] and Fiorino [7] to study the difference between the buildings adopting steel-concrete floors and OSB-sheathed composite floors, and the CFS strap-braced walls were used to resist the seismic force. It should be emphasized that the strap-braced wall is one common CFS seismic force resisting system [8], and it could be more economical compared with shear walls sheathed with steel plates. Guan and Shi et al. [9] conducted shake table tests and nonlinear finite element analyses on a full-scale single-storey prefabricated sheathed CFS building, in which the composite wall with short diagonal bracings and OSB sheathing was adopted as the horizontal lateral force resisting member. They also proposed more applicable seismic construction measures for CFS structures. The above mentioned studies all focused on low-rise CFS structure buildings, and

\* Correspondence to: No. 83 Shabeijie, Shapingba, Chongqing, 400044, China.

E-mail address: [shiyucivil@cqu.edu.cn](mailto:shiyucivil@cqu.edu.cn) (Y. Shi).

the horizontal lateral force resisting members were typical lightweight wallboard sheathed composite walls.

As we know, the stiffness and strength of lightweight wallboard sheathed composite walls are very important for the seismic behavior of CFS buildings, which were affected by sheathing materials, sheathing-fastener connection stiffness and strength. Selvaraj et al. [10–14] have done a series of detailed studies on the sheathing-fastener connection in cold-formed steel wall panels, which formulated the criteria and parameters for the selection of the sheathing for the construction of the CFS framed wall panel, explored the bracing effect of fastener-connection on point-symmetric CFS stud provided at the fastener connection, investigated the sheathing-fastener connection failures and proposed two design methods for sheathed CFS structural members.

With the development of the CFS structure, it is gradually applied in multi-storey buildings. However, the applicability and safety of multi-storey CFS structure buildings in seismic areas need to be explored. At present, studies on multi-storey CFS structures mainly adopt numerical simulation methods, while experimental data on large-scale structures examined through shake table tests are limited. Wang and Hutchinson et al. [15–17] conducted shake table tests to evaluate the seismic performance of full-scale six-storey prefabricated CFS shear wall structure buildings. The shear wall was composed of a 16 mm gypsum board bonded with a 0.686 mm steel plate as the wall panel. Building on this foundation, the post-earthquake fire testing was performed. The global response, physical damage, shear wall behavior, and design implications were investigated. In addition, Ye et al. [18,19] conducted a shake table test on a 1:2 scaled five-storey prefabricated CFS composite shear wall structure building, in which the end columns of the shear wall were CFS composite members filled with concrete to form concrete-filled steel tubular columns, and the building adopted CFS-concrete composite floors.

In the above two studies, flat steel plate shear walls with excellent lateral performance were used as the horizontal lateral force resisting members to satisfy the high requirements of multi-storey CFS structures. In addition, many experimental and theoretical researches have been conducted on the corrugated plate shear walls. Qiu et al. [20,21] studied the elastic buckling, shear strength and post-peak behavior of trapezoidally corrugated wall plates in steel plate shear walls. Zhang et al. [22,23] found that with proper slit configurations on the sheathing, CFS shear walls sheathed with corrugated steel sheets with slits presented an improved high ductility without significant reduction in shear strength and stiffness. To improve the ductility of the corrugated sheet-sheathed CFS shear walls, a special energy dissipation bracing was developed by Yu et al. [24] to provide additional stiffness and lateral resistance strength immediately in the postpeak stage. And the test results showed that installing the proposed energy dissipation bracing can be an efficient approach to enhance the seismic performance of CFS-framed shear walls. The above studies showed that, except for flat steel plate shear walls, the corrugated plate shear walls could also be adopted as lateral force resisting components in multi-storey CFS buildings.

Although the above researchers have conducted a series of shake table tests on CFS structure buildings, investigations on the system-level seismic performance of CFS buildings are still insufficient, particularly for multi-storey buildings. In addition, practical buildings were usually affected by bidirectional ground motion in the horizontal direction, the torsional effects of buildings under unidirectional and bidirectional earthquake actions were different, and then the global seismic responses of buildings were also different. However, shake table tests considering the impact of real bidirectional earthquake action on the seismic performance of multi-storey CFS structures have not been conducted. Thus, in this study, a multi-storey CFS-SPSWS was first proposed, and then the shake table test program of the six-storey full-scale CFS-SPSWS buildings was considered in detail. This shake table test is the first experimental research of full-scale six-storey CFS structures under bidirectional ground motion input in the world, and

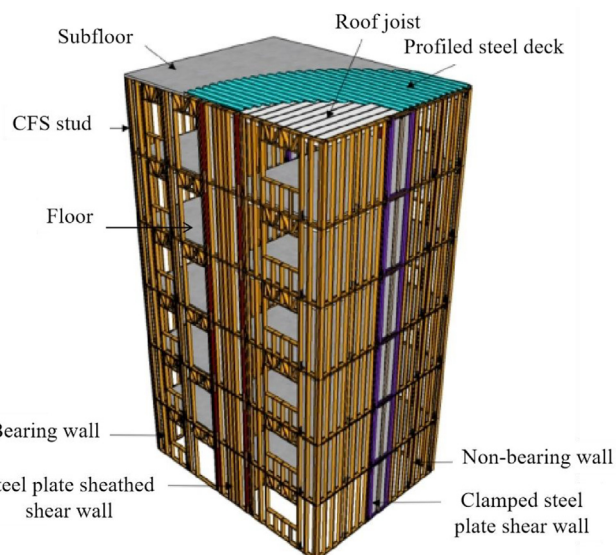


Fig. 1. Multi-storey CFS-SPSWS system.

the magnitude of height to width ratio of this tested model is also the largest. The failure features, natural frequency, strains of structural members, acceleration response, and displacement response were obtained, and the influences of nonstructural members on the seismic performance of the structure were analyzed.

## 2. Multi-storey CFS-SPSWS system

The multi-storey CFS-SPSWS system consists of shear walls, bearing walls, non-bearing walls, floors, and roofs, as shown in Fig. 1. This system relies on shear walls to resist horizontal wind loads and seismic loads.

In this study, the shear walls included the CFS-clamped steel plate shear walls and CFS-steel plate sheathed shear walls. The CFS-clamped steel plate shear wall, as shown in Fig. 2(a), uses the surrounding edge components to clamp the thin steel plate, and the two end columns and the top and bottom beams are closely connected with the steel plate through self-tapping screws. The column-beam joints are connected by connecting steel plates through bolts. The hold-downs are arranged at four corners of the wall and connected with the end columns through bolts. The tensile field and post-buckling strength of the thin steel plate can be fully utilized to resist horizontal loads. The CFS-clamped steel plate shear wall has the advantages of a high bearing capacity, large lateral stiffness, and excellent energy dissipation [25]. The CFS-steel plate sheathed shear walls, as shown in Fig. 2(b), used in multi-storey CFS-SPSWS systems should avoid the buckling of end columns caused by the excessive overturning moment. Therefore, CFS square steel pipe end columns are used as end studs to replace the traditional built-up CFS members. The steel plates are connected with studs through self-tapping screws.

In the multi-storey CFS-SPSWS system, the composite floors or roofs consist of CFS joists, profiled steel decks, and slabs. The materials for slabs can be lightweight concrete, gypsum-based self-leveling underlayment, or cement fiber boards (CFBs). The floor and roof adopt ledger framing [26] in the multi-storey CFS-SPSWS system buildings. The connection details between floor joists and wall studs are shown in Fig. 3(a) and (b). The U-shaped ledger tracks are installed on the inside face of the wall studs, and the C-shaped joists are connected to the track with self-tapping screws through clip angles. The tracks between the upper and lower walls are directly connected through screws, and the end joist is screwed to each wall stud as shown in Fig. 3(b).

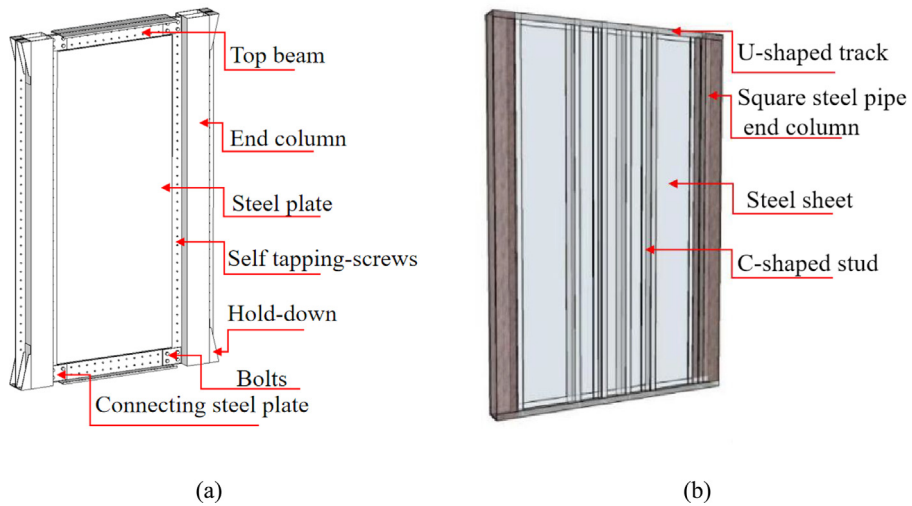


Fig. 2. Shear walls. (a) CFS-clamped steel plate shear wall. (b) CFS-steel plate sheathed shear wall.

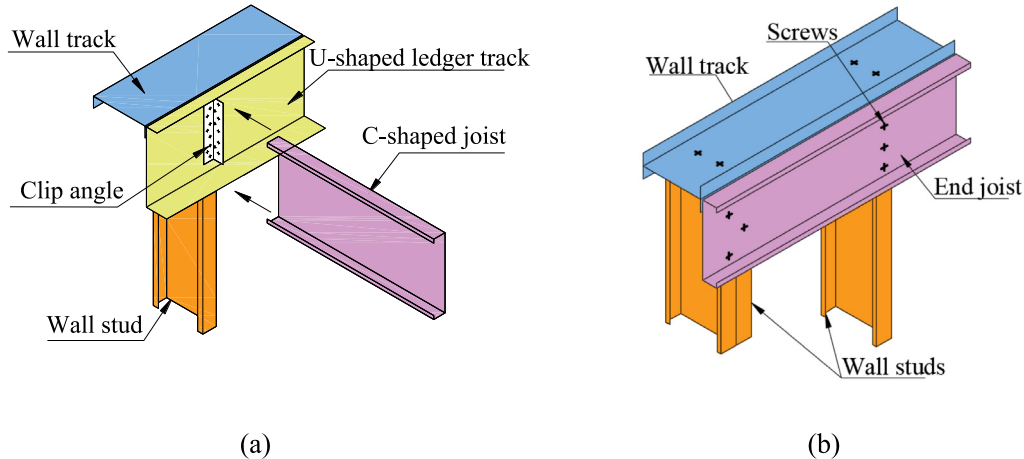


Fig. 3. Ledger framing. (a) Connection of U-shaped ledger track. (b) Connection of end joist.

**Table 1**  
Material properties of building members.

Members	Section dimension/mm	Yield strength/MPa	Tensile strength/MPa	Elastic modulus/MPa
Square steel pipe columns	□152 × 152 × 6	307.8	426.3	227621.7
C-shaped studs	C152 × 41 × 11 × 1.2	343.8	462.6	209087.8
U-shaped tracks	U152 × 41 × 1.2			
Steel plate of SW-1	2700 × 1800 × 0.8	367.5	487.1	202638.7
Cap-shaped end columns	Ω120 × 70 × 40 × 2.5	263.3	340.0	201869.7
U-shaped beams	U104 × 70 × 2.5			
Vertical stiffeners	Ω90 × 70 × 30 × 10 × 1.5	267.4	357.5	204106.7
Steel plate of SW-A	2700 × 1210 × 0.8	272.7	366.9	197830.8
C-shaped joists	C254 × 41 × 11 × 1.8	348.6	469.8	211712.2
U-shaped joists	U254 × 41 × 1.8			
Profiled steel deck	YX820 × 14 × 0.8	272.7	366.9	197830.8

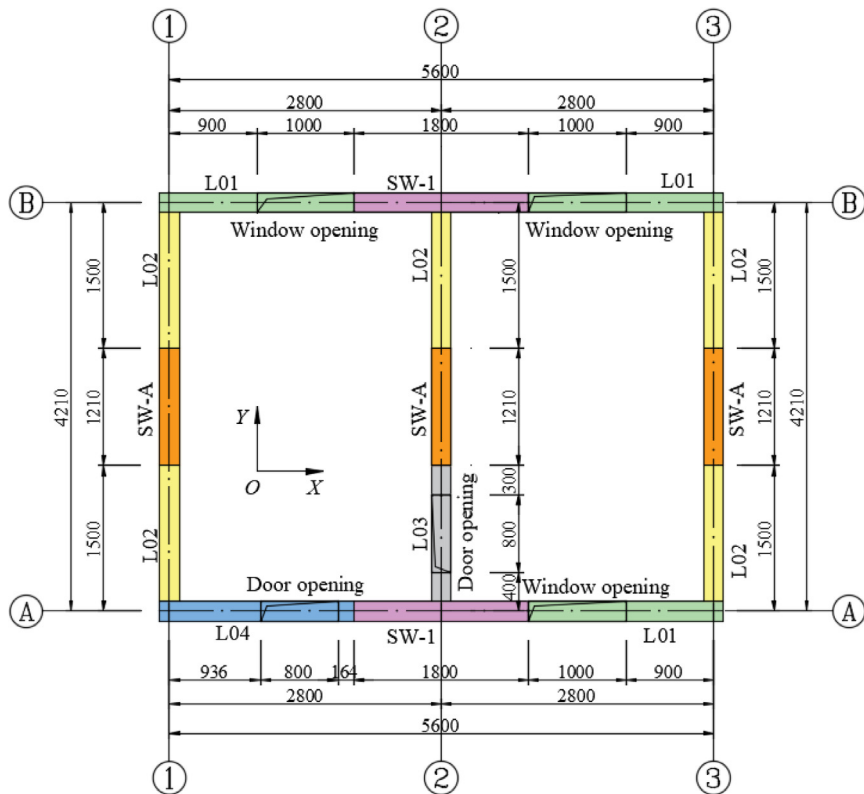
This new multi-storey CFS-SPSWS system has been used in practice in Shandong and Hubei provinces in China. But since the mechanical performance of CFS-clamped steel plate shear wall has not been fully studied, only the CFS-steel plate sheathed shear wall was used as the seismic force-resisting system in the above practice engineering.

### 3. Test overview

#### 3.1. Model design

The six-storey CFS-SPSWS structure model had a floor height of 2700 mm, longitudinal length of 5600 mm, and transverse width of

4210 mm. The plane layout is shown in Fig. 4(a). In this figure, the two horizontal axes along the X-direction are defined as axis A and axis B respectively, and the three vertical axes along the Y-direction are defined as axis ①, axis ②, and axis ③ respectively. To better observe the lateral force contribution of the shear wall in each axis, the shear walls were arranged in the middle of each axis rather than the corner to avoid the interaction between the shear walls in two directions at the corner. In the X- and Y-directions, CFS-steel plate sheathed shear walls (marked as SW-1) and CFS-clamped steel plate shear walls (marked as SW-A) were employed respectively to resist the horizontal lateral force. Walls L01 and L04 were the bearing walls, and the C-shaped joists



(a)



(b)

**Fig. 4.** Details of model design. (a) Building plan layout. (b) Building composition.

**Table 2**  
Shear stiffness of screw connections.

Screw	Member 1	Member 2	Screw spacing (mm)	Shear stiffness (kN/mm)
ST4.8	12 mm gypsum board	C152 × 41 × 11 × 1.2	150	1.35
ST4.8	12 mm CFB	C152 × 41 × 11 × 1.2	150	2.83
ST5.5	YX820 × 14 × 0.8 profiled steel deck	C254 × 41 × 11 × 1.8	126	4.40
ST4.8	0.8 mm steel plate of SW-1	□152 × 152 × 6	150	4.77
ST5.5	0.8 mm steel plate of SW-A	Ω120 × 70 × 40 × 2.5	50	2.54

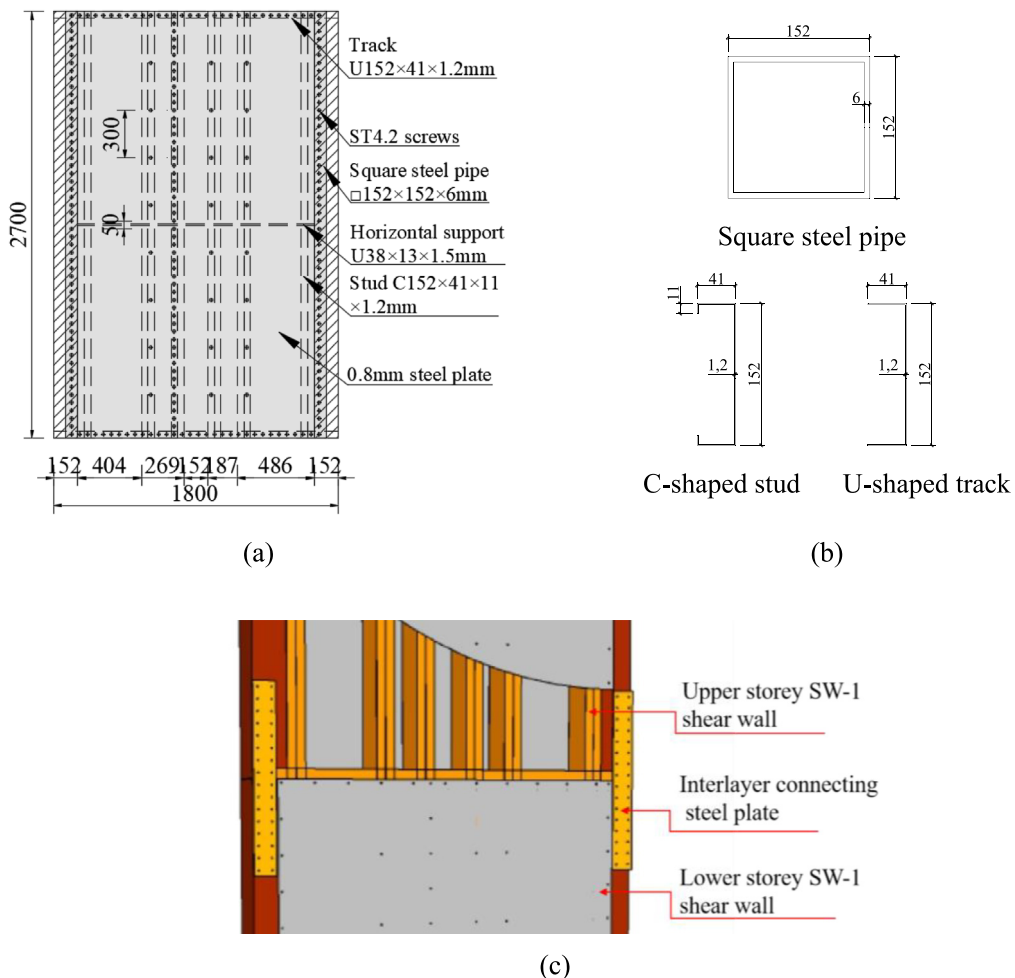


Fig. 5. Diagram of SW-1. (a) Screw connection. (b) Section dimensions. (c) Interlayer connection of SW-1.

were hung from the bearing walls. Walls L02 and L03 were the non-bearing walls. Moreover, the door and window opening sizes were 2100 (height)  $\times$  800 mm (width) and 1200 (height)  $\times$  1000 mm (width), respectively. The bottom U-shaped tracks of the first-floor walls were connected with the hot-rolled steel beam base using high-strength bolts, and the steel beam base was fixed on the shake table as shown in Fig. 4(b).

SW-1 shown in Fig. 5(a) comprised two square steel pipe end columns with the dimensions of  $\square 152 \times 152 \times 6$  mm, CFS studs of  $C152 \times 41 \times 11 \times 1.2$  mm spaced at 400 mm, tracks of  $U152 \times 41 \times 1.2$  mm, and steel plates with a thickness of 0.8 mm. The horizontal supports of  $U38 \times 13 \times 1.5$  mm were set at the middle height of the SW-1 shear walls. The detailed dimensions of the steel members are presented in Fig. 5(b). For SW-1 from the first to the fourth floor, the double-sheathed steel plates were connected to the steel frame using self-tapping screws with a diameter of 4.8 mm (ST4.8) spaced at 50 mm and 300 mm along the perimeter and in the field (50/300 mm) of the steel plate, respectively. At the fifth and sixth floors, SW-1 was single-sheathed, and the screw spacings were 50/300 and 150/300 mm, respectively. Interlayer connecting steel plates were screwed or welded to the upper and lower steel square pipe columns to transfer the uplift force, as shown in Fig. 5(c).

SW-A consisted of CFS cap-shaped end columns with dimensions of  $\Omega120 \times 70 \times 40 \times 2.5$  mm, U-shaped beams with dimensions of  $U104 \times 70 \times 2.5$  mm, vertical stiffeners with dimensions of  $\Omega90 \times 70 \times 30 \times 10 \times 1.5$  mm, and a steel plate with a thickness of 0.8 mm, as shown in Fig. 6(a). The edge members and vertical stiffeners were connected with the steel plate with ST5.5 screws spaced at 50 mm.

Connecting steel plates were used to connect the cap-shaped end column and the U-shaped beam through bolts. L-shaped clip angles were used to connect the vertical stiffener with the U-shaped beam using ST5.5 screws. The section shapes and dimensions of the cap-shaped end columns, U-shaped beams, vertical stiffeners, connecting steel plates, and L-shaped clip angles are presented in Fig. 6(b). The bottom U-shaped beam of the upper storey SW-A shear wall was connected with the upper U-shaped beam of the lower storey SW-A shear wall using four M27 pull-out bolts and fourteen M12 shear bolts. The shear bolt spacing was 100 mm, as shown in Fig. 6(c).

The diagrams of L01, L02, L03 and L04 are shown in Figs. 7(a) and 7(b). The stud spacing in the bearing and non-bearing walls was 400 mm. The dimensions of the C-shaped column and U-shaped track were the same as those of the SW-1 shear wall.  $U38 \times 13 \times 1.5$  mm horizontal supports were set at the middle height of the wall, and  $L38 \times 38 \times 1.5$  mm clip angles were used to connect with the columns through the ST4.8 screws, as shown in Fig. 7(c). Hold-downs were connected with the two ends of the studs at the T-shaped and L-shaped corners and door and window openings, as presented in Fig. 7(d). Two rows of ST4.8 screws, with a screw spacing of 300 mm, were used to connect the upper and lower wall tracks to transfer the horizontal shear force.

The floors and roofs comprised a CFS frame, profiled steel decks and 18 mm thick medium density CFBs. Fig. 8(a) shows that the CFS frame of floors consists of C-shaped joists with dimensions of  $C254 \times 41 \times 11 \times 1.8$  mm spaced at 400 mm on center, and U-shaped ledger tracks with dimensions of  $U254 \times 41 \times 1.8$  mm connected to the flange at each end of the C-shaped joists through ST4.8 screws. Moreover,

**Table 3**  
Summary of the test plan for the first stage model.

Test number	Case label	Earthquake intensity	Ground motion	Main direction	PGA/g X	Y
1	WN1	White noise			0.05	0.05
2	S8WLXY			X	0.070	0.047
3	S8WLYX		Wolong	Y	0.047	0.070
4	S8EIXY			X	0.070	0.044
5	S8EIYX	FOE8	El Centro	Y	0.044	0.070
6	S8RGX			X	0.070	–
7	S8RGY			Y	–	0.070
8	S8RGXY		Artificial	X	0.070	0.060
9	S8RGYX			Y	0.060	0.070
10	WN2	White noise			0.050	0.050
11	M7WLXY		Wolong	X	0.100	0.067
12	M7WLYX			Y	0.067	0.100
13	M7EIXY		El Centro	X	0.100	0.062
14	M7EIYX	DBE7		Y	0.062	0.100
15	M7RGX			X	0.100	–
16	M7RGY			Y	–	0.100
17	M7RGXY		Artificial	X	0.100	0.085
18	M7RGYX			Y	0.085	0.100
19	WN3	White noise			0.050	0.050

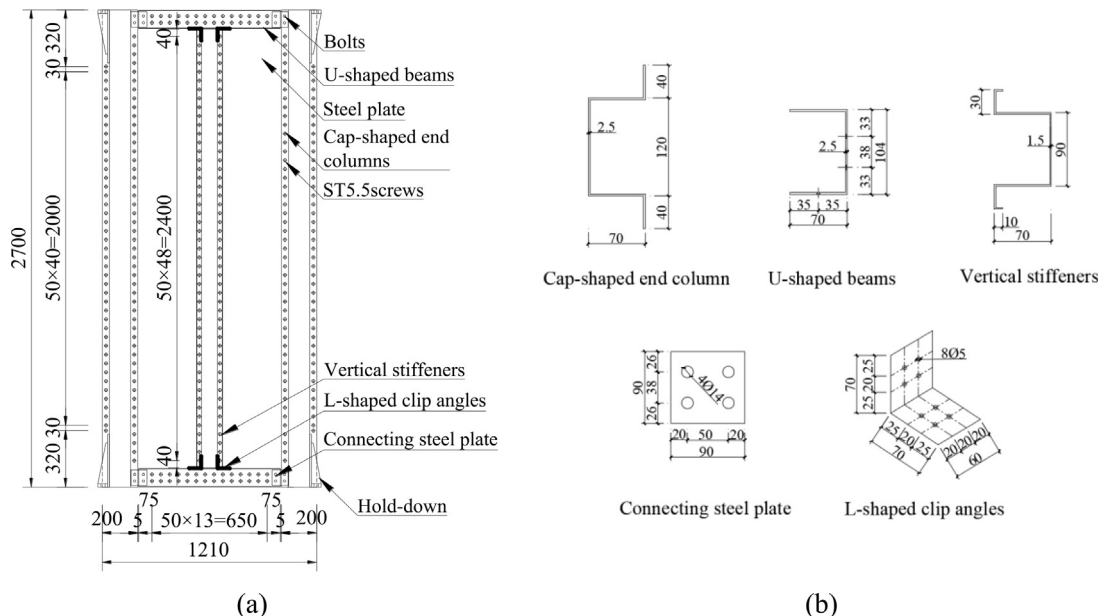


**Fig. 6.** Diagram of SW-A. (a) Screw connection. (b) Section dimensions of steel members. (c) Interlayer connection of SW-A.

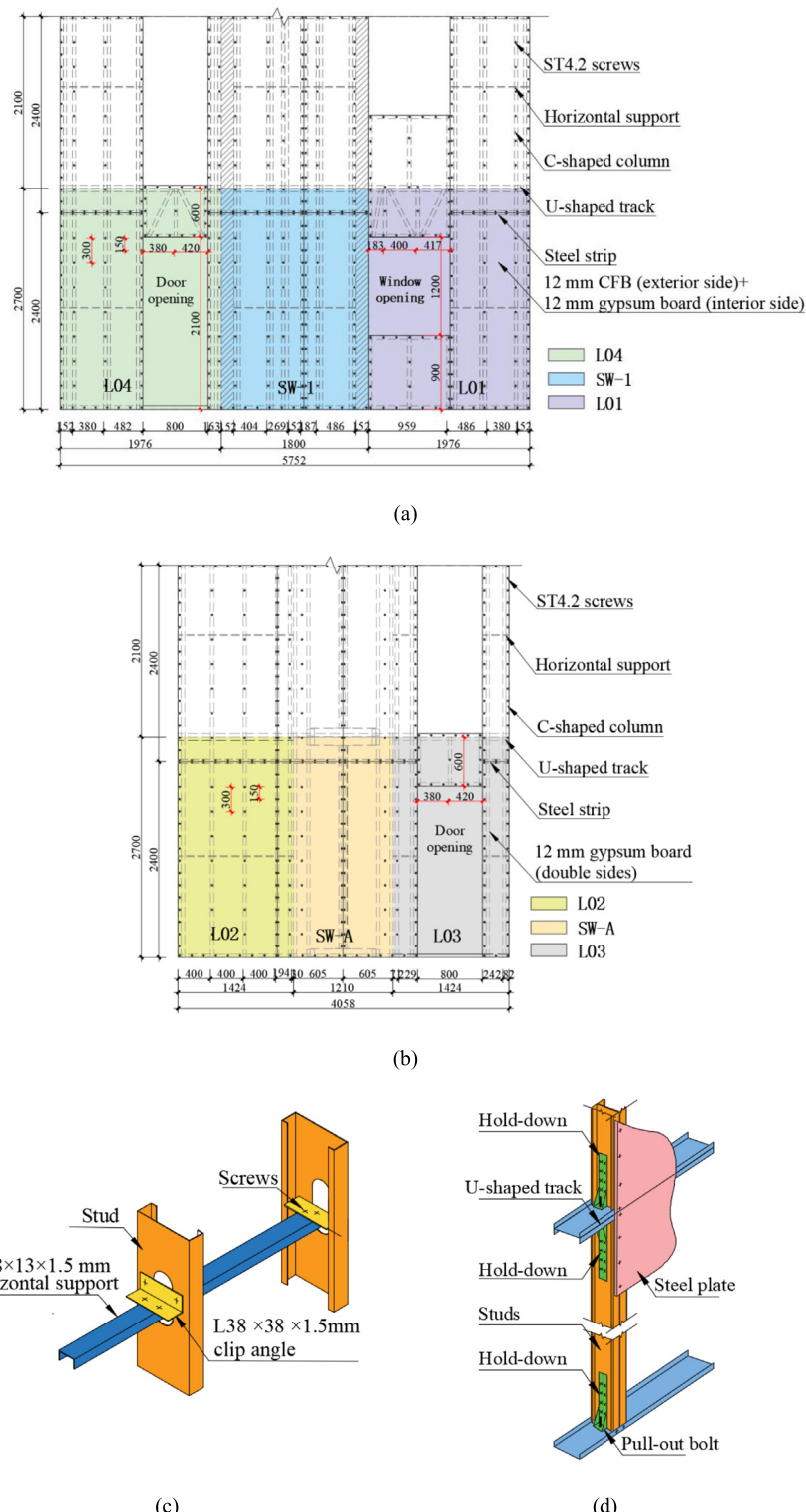
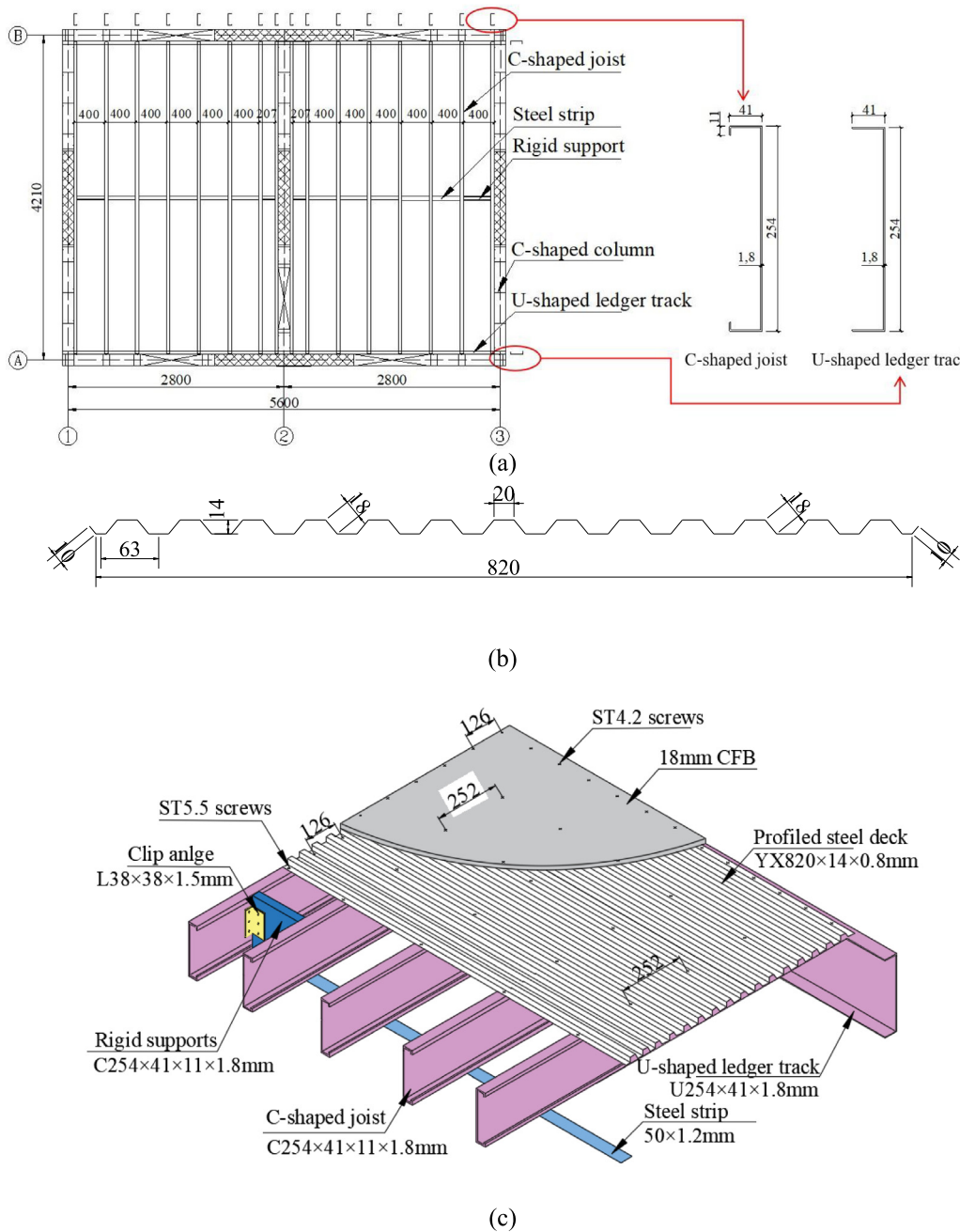


Fig. 7. Structural details of bearing and non-bearing walls. (a) Screw location of A-axis. (b) Screw location of ②-axis. (c) Horizontal supports. (d) Hold-downs.

the web of the C-shaped joists was connected to the web of the U-shaped ledger tracks with clip angles of L 42 × 42 × 215 × 1.8 mm, as shown in Fig. 3(a). The section dimensions of the profiled steel deck are shown in Fig. 8(b). The profiled steel deck was connected with the upper flange of the joist through ST5.5 screws, and the screw spacing was 126 mm/252 mm. The CFB was connected with the profiled steel deck and upper flange of the joists through ST4.2 screws, and the screw spacing was 126 mm/252 mm. The steel strip of 50 × 12 mm was set

at the bottom flange in the middle of the joist span. Rigid supports of C 254 × 41 × 11 × 1.8 mm were arranged at both ends of the steel strip and connected with the floor joists on both sides through clip angles. The connection details of floors are shown in Fig. 8(c).

To investigate the influence of the nonstructural members on the seismic performance of multi-storey CFS-SPSWS buildings, the shake table tests included two stages. Fig. 9(a) shows the first stage test model, which only includes the structural components: CFS-clamped



**Fig. 8.** Diagram of floors and roofs. (a) Joist layout. (b) Section dimensions of steel members. (c) Connection Details.

steel plate shear walls, CFS-steel plate sheathed shear walls, steel framing of bearing and non-bearing walls, floor joists, profiled steel decks, and CFBs. Based on the first stage model, for the second stage test model, as shown in Fig. 9(b), 12 mm thick CFBs were sheathed on the outside of the A- and B-axis walls through ST4.2 screws, and 12 mm thick gypsum boards were sheathed on the inside of the A- and B-axis walls and on both the inside and outside of the other walls with ST4.2 screws. The screw spacings in the CFB and gypsum board were 150 mm/300 mm. The diagrams of screw locations are presented in Figs. 7(a) and 7(b).

The steel material characteristics are presented in Table 1. Through monotonic shear loading tests, the shear stiffnesses of screw connections are shown in Table 2.

### 3.2. Instrumentation

In the tests, acceleration sensors and stay wire displacement sensors were arranged to measure the dynamic characteristics and displacement response of the building. The displacement of each acceleration measuring point can be obtained using the acceleration quadratic integral method, and the stay wire displacement sensors were only arranged at the third and the sixth floors to compare and correct the accuracy of the displacement obtained by quadratic integration of acceleration. The definitions of D3-X and A3-1-XY are shown in Fig. 10. Considering the elevation of the third floor as an example, the acceleration measuring point A3-1-XY presented in Fig. 10 at the center of the floor was used to measure the horizontal acceleration of the third floor, and the other acceleration measuring points were used

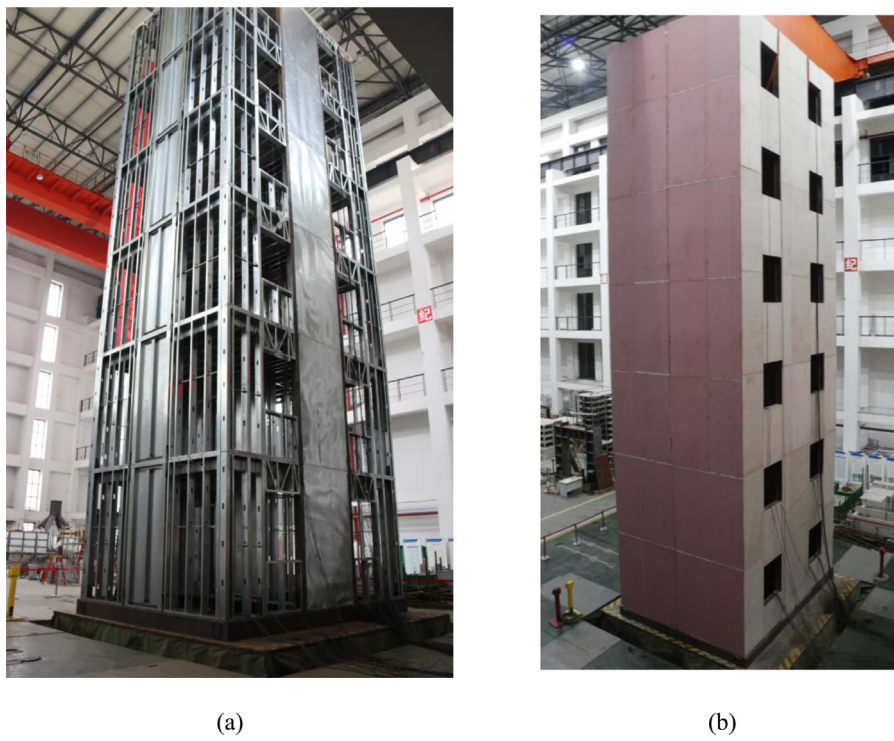


**Fig. 9.** Shake table test models. (a) First stage model. (b) Second stage model.

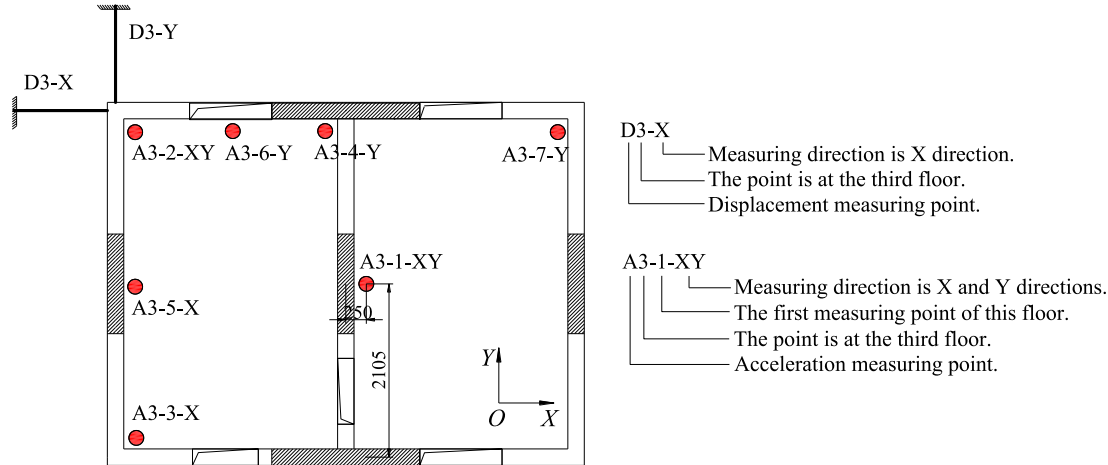


**Fig. 10.** Layout of sensor measuring points.

to calculate the torsional deformation of the structure and evaluate the rigidity of the floor. Moreover, strain points were arranged at the end studs of the shear walls, bearing walls, and non-bearing walls at the first and second floors to compare the mechanical characteristics of the lateral force resisting members with these of non-lateral force resisting members under various test conditions.

### 3.3. Loading scheme

According to the Chinese standards including the load code for the design of building structures (GB 50009-2012) [27] and the code for seismic design of buildings (GB 50011-2010) [28], the live loads of floors and the roof for residential buildings were 2 kN/m<sup>2</sup> and 0.5 kN/m<sup>2</sup>, respectively. When the earthquake action was considered, these two live loads should be multiplied by the combination coefficient of 0.5 in calculating the seismic weight load according to GB 50011-2010 [28]. Therefore, the additional mass considering the roof and

floor live loads was approximately 11.28 t. Moreover, to compare the test results of the two stages models, it was ensured that the weights of the models in the two tests were equal. Therefore, in the first stage model, a wall panel counterweight of 1.27 t was arranged on each floor. According to GB 50011-2010 [28], the ground motion records of the Wolong earthquake, El Centro earthquake, and two artificial earthquake waves were selected as the input excitations, and the acceleration time histories for the two test directions are presented in Fig. 11. The acceleration spectrums of the ground motions and the codified design response spectrum curve are shown in Fig. 12. It can be seen that the seismic response spectrum and design response spectrum are in good agreement in the corresponding period of the structure.

To avoid the component damage in the loading process of the first stage model, the peak ground accelerations (PGAs) of the input seismic wave of the first stage model included 0.070 g (frequently occurring earthquake with a PGA of 0.07 g at an intensity level of 8 degree (FOE8)) and 0.10 g (design basis earthquake with a PGA of 0.10 g at an

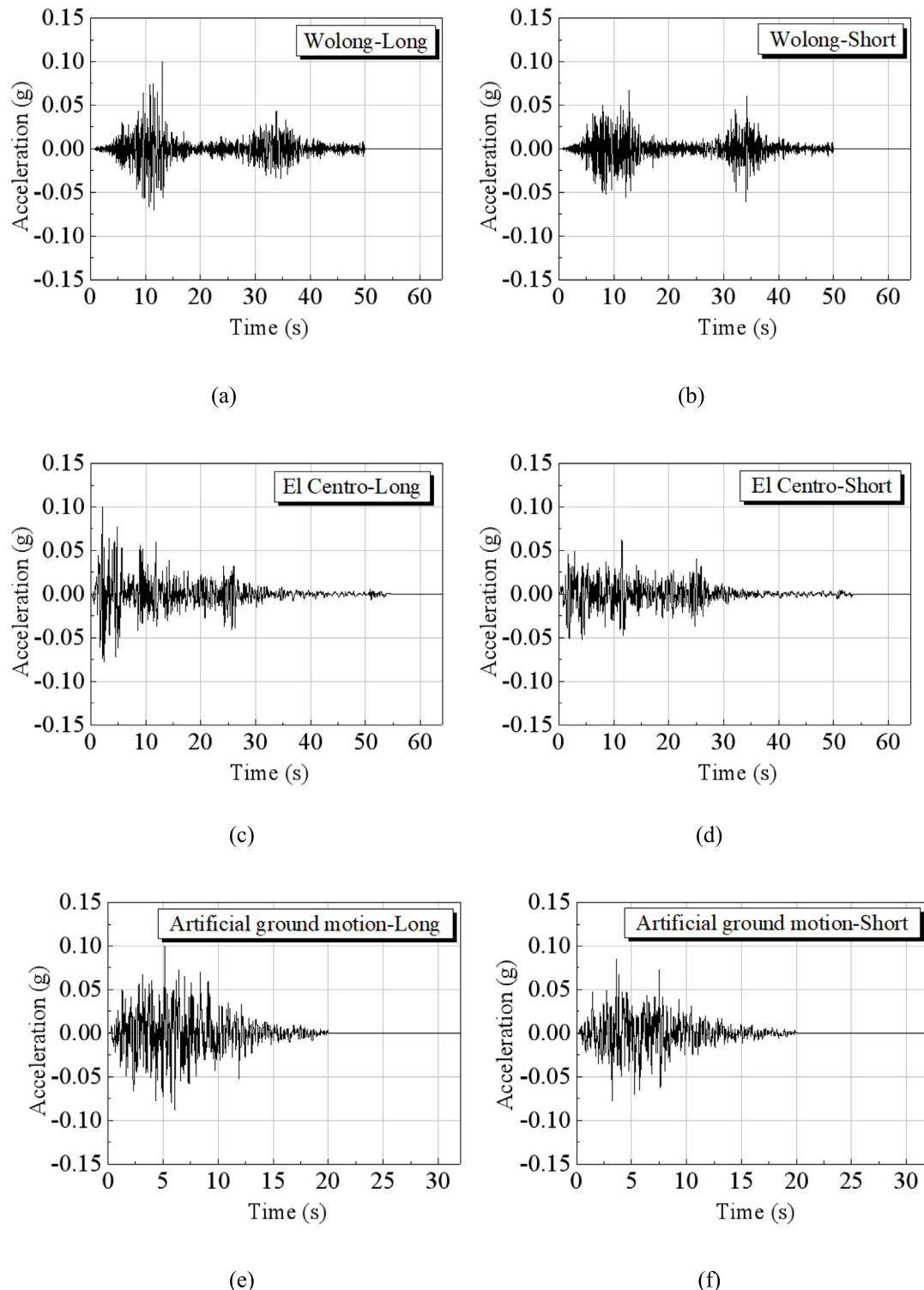


**Fig. 11.** Acceleration time histories of the three ground motions. (a) Wolong ground motion in the long direction. (b) Wolong ground motion in the short direction. (c) El Centro ground motion in the long direction. (d) El Centro ground motion in the short direction. (e) Artificial ground motion in the long direction. (f) Artificial ground motion in the short direction.

intensity level of 7 degree (DBE7)), with a total of 19 cases, as shown in Table 3.

For the second stage model, the PGA included 0.07 g (FOE8), 0.1 g (DBE7), 0.14 g (FOE9), 0.20 g (DBE8), 0.22 g (maximum considered earthquake with a PGA of 0.220 g at an intensity level of 7 degree

(MCE7)), 0.30 g (DBE8.5), and 0.40 g (MCE8), with a total of 53 cases, as shown in Table 4.

Under the seismic intensity of each magnitude, bidirectional Wolong, bidirectional El Centro, unidirectional artificial, and bidirectional artificial waves were successively used as the input. In the bidirectional input cases, the X- and Y-directions were the primary and secondary

**Table 4**  
Summary of the test plan for the second stage model.

Test number	Case label	Earthquake intensity	Ground motion	Main direction	PGA/g
				X	Y
1	WN1	White noise			0.05 0.05
2	S8WLXY			X	0.070 0.047
3	S8WLYX		Wolong	Y	0.047 0.070
4	S8EIXY			X	0.070 0.044
5	S8EIYX	FOE8	El Centro	Y	0.044 0.070
6	S8RGX			X	0.070 –
7	S8RGY			Y	– 0.070
8	S8RGXY		Artificial	X	0.070 0.060
9	S8RGYX			Y	0.060 0.070
10	WN2	White noise			0.050 0.050
11	M7WLXY			X	0.100 0.067
12	M7WLYX		Wolong	Y	0.067 0.100
13	M7EIXY			X	0.100 0.062
14	M7EIYX	DBE7	El Centro	Y	0.062 0.100
15	M7RGX			X	0.100 –
16	M7RGY			Y	– 0.100
17	M7RGXY		Artificial	X	0.100 0.085
18	M7RGYX			Y	0.085 0.100
19	WN3	White noise			0.050 0.050
20	S9WLXY			X	0.140 0.093
21	S9WLYX		Wolong	Y	0.093 0.140
22	S9EIXY			X	0.140 0.087
23	S9EIYX	FOE9	El Centro	Y	0.087 0.140
24	S9RGX			X	0.140 –
25	S9RGY			Y	– 0.140
26	S9RGXY		Artificial	X	0.140 0.119
27	S9RGYX			Y	0.119 0.140
28	WN4	White noise			0.050 0.050
29	M8WLXY			X	0.200 0.134
30	M8WLYX		Wolong	Y	0.134 0.200
31	M8EIXY			X	0.200 0.124
32	M8EIYX	DBE8	El Centro	Y	0.124 0.200
33	M8RGX			X	0.200 –
34	M8RGY			Y	– 0.200
35	M8RGXY		Artificial	X	0.200 0.170
36	M8RGYX			Y	0.170 0.200
37	WN5	White noise			0.050 0.050
38	G7WLXY			X	0.220 0.147
39	G7WLYX		Wolong	Y	0.147 0.220
40	G7EIXY	MCE7		X	0.220 0.137
41	G7EIYX		El Centro	Y	0.137 0.220
42	G7RGXY			X	0.220 0.187
43	G7RGYX		Artificial	Y	0.187 0.220
44	WN6	White noise			0.050 0.050
45	M8.5WLYX			Y	0.200 0.300
46	M8.5EIYX		El Centro	Y	0.187 0.300
47	M8.5RGXY	DBE8.5		X	0.300 0.255
48	M8.5RGYX		Artificial	Y	0.255 0.300
49	WN7	White noise			0.050 0.050
50	G8RGYX			Y	0.340 0.400
51	G8RGXY	MCE8	Artificial	X	0.400 0.340
52	G8WLYX		Wolong	Y	0.267 0.400
53	WN8	White noise			0.050 0.050

directions, respectively, and then they were interchanged. When the PGA exceeded 0.2 g, the unidirectional artificial wave condition was abandoned to reduce the cumulative damage of the building. When the PGA was 0.4 g, the El Centro wave was not loaded owing to the limited capacity of the shake table. Before the test and after the end of each level of loading cases, bidirectional white noise frequency scanning was conducted to obtain the frequencies of the structure in X - direction and Y - direction and to monitor the stiffness change in the building after experiencing the earthquakes of different intensities.

#### 4. Failure characteristics

##### 4.1. First stage model

During the test, the deformations at the first floor of the model were significant; thus, the failure phenomenon at only the first storey was considered. In the first stage, with an increase in the input PGA, the overall shaking of the building and the bulging deformation of the steel plate shear walls gradually increased under the seismic load.

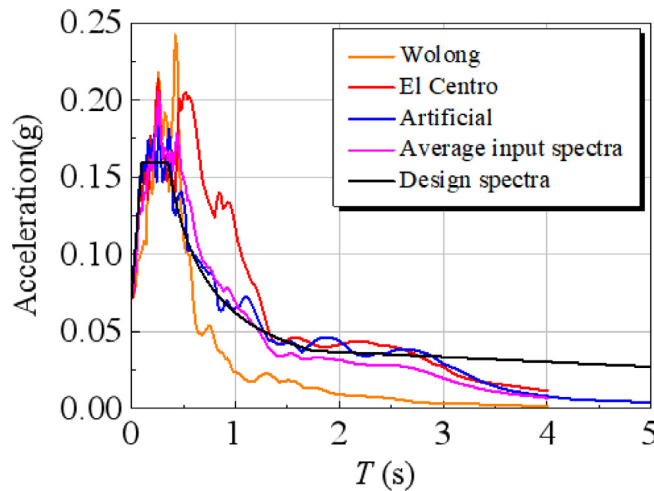


Fig. 12. Input ground motion response spectrums vs. design spectrum.



Fig. 13. Failure characteristics of the first stage model. (a) Drawing out of self-tapping screw of steel plate in shear wall. (b) CFB cracks in the floor.

After the cases with a PGA of 0.10 g, three intermediate screws of axis  $B$  that connected the steel plate and steel stud fell off, as shown in Fig. 13(a). This is because the screw spacing around the steel stud was 50 mm, which had a strong buckling restraint effect on the steel plate, and the buckling deformation of the steel plate corner was large. However, the intermediate screw spacing was 300 mm, and the buckling deformation constraint on the steel plate was relatively small, and thus, the bulging deformation of the steel plate produced a warping force on the intermediate screw to pull it out of the C-shaped column. After the loading, longitudinal cracks were observed at the corners of the small long strip floor CFB in contact with the surrounding wall and the corners of the entire CFB in contact with the shear wall, as shown in Fig. 13(b). The vibration response of the model in the Y-direction was significantly larger than that in the X-direction, which was related to the weak lateral stiffness in the Y-direction. The seismic response of the model under the El Centro, artificial, and Wolong waves decreased successively.

#### 4.2. Second stage model

Compared with the corresponding working conditions for the first stage model, the overall shaking of the second stage model was significantly weakened, but the seismic response in the Y-direction was larger than that in the X-direction. The failure feature in this phase was the screw connection failure in the light wall panel. With an increase in the PGA, the order of the wall panel failure positions was

as follows: the corners of the door and window openings, shear walls and corners of the structure, and the field of the wall panel. When the PGA was small, some corners of gypsum boards were pressed and then crushed, and small cracks appeared in the CFBs. Due to the interaction between screws and wall panels, the screw holes at the gypsum board gradually become bigger, screws began to tilt, and cracks initiated in the gypsum board close to the screws. Besides, the cracks in the CFBs gradually extended and expanded. After the cases with a PGA of 0.20 g, new cracks appeared in the CFBs at the L-shaped corner connecting axis  $B$  and axis ③, as shown in Fig. 14(a), and the number of loose screws around the door and window openings increased, as shown in Fig. 14(b). The internal self-tapping screw holes of the gypsum board in axis  $B$  were damaged, and some screws were inclined, as shown in Fig. 14(c). After the cases with a PGA of 0.40 g, the gypsum board around the screw hole at the corner of the gypsum board outside axis ① was crushed, as shown in Fig. 14(d), middle screws of the gypsum board outside axis ③ were inclined and concaved, and nail holes were seriously damaged. Five screws inside the CFB outside axis  $A$  were inclined, as shown in Fig. 14(e). The screw connections at the gypsum board and CFB were seriously damaged, and the diaphragm effect was invalid. After the test, it was observed that there was a corner fracture in the CFBs of the third and sixth floors, as shown in Fig. 14(f). The wall panels of floors 2–6 had no significant cracking, and the damage degree of the screw connection was considerably lower than that of the first floor. After the steel plate shear wall on the first floor was removed, it was found that the shear bolt hole at the U-shaped beam exhibited a pressure bearing deformation, as shown in Fig. 14(g).



**Fig. 14.** Failure characteristics of the second stage model. (a) Corner crack of CFBs. (b) Loose screws around doors and windows. (c) Damaged internal screws of the gypsum board. (d) Damage of screw connection at the edge of the gypsum board in axis ①. (e) Damage of the gypsum board and internal screws in axis ③. (f) CFB cracking of floors. (g) The pressure bearing deformation of bolt hole at the U-shaped beam.

In summary, the failure characteristics of the building model under the earthquake with a PGA of 0.40 g included the peripheral screw connection failure of the wall panel. With an increase in the ground motion intensity, the damage of the wall panels gradually intensified, the diaphragm effect weakened, and the shear force borne by the steel plate shear wall gradually increased. However, the structural members were not damaged, and the structure was not in danger of collapse.

## 5. Test results and discussions

### 5.1. Structural dynamic characteristics

The transfer function curves were obtained from the white noise random wave, where the real part of the complex variable is zero, and

**Table 5**  
Dynamic characteristic results of test models.

Experimental stage	Case label	Natural vibration frequency (Hz)		The percentage of the stiffness degradation (%)	
		$f_x$	$f_y$	X-direction	Y-direction
First stage	WN1	2.00	1.19	–	–
	WN2	1.88	1.13	11.64	9.83
	WN3	1.87	1.12	12.58	11.42
Second stage	WN1	2.68	2.38	–	–
	WN2	2.63	2.00	3.70	29.38
	WN3	2.56	1.75	8.75	45.93
	WN4	2.51	1.69	12.28	49.58
	WN5	2.44	1.51	17.11	59.75
	WN6	2.37	1.38	21.80	66.38
	WN7	2.31	1.25	25.71	72.42
	WN8	2.30	1.19	26.35	75.00

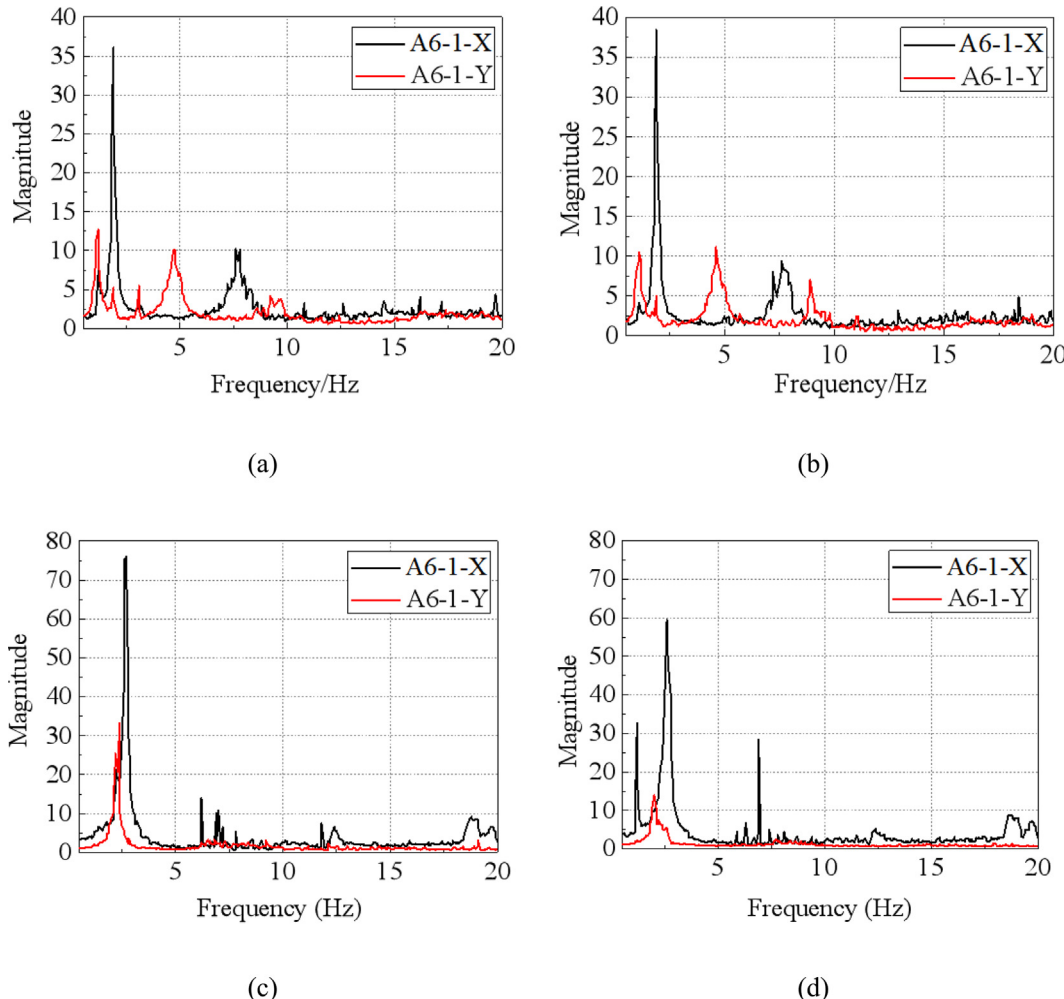


**Fig. 15.** Transfer function curves in terms of the fundamental frequency. (a) WN1 of the first stage model. (b) WN2 of the first stage model. (c) WN1 of the second stage model. (d) WN2 of the second stage model.

the imaginary part is the angular frequency, which is the natural frequency. The transfer function curves of the first stage model including WN1 and WN2, and those of the second stage model including WN1 and WN2 are presented in Fig. 15.

The calculation results of the dynamic characteristics of the building are presented in Table 5, where  $f_x$  and  $f_y$  are the natural frequencies in the X- and Y-directions, respectively. Eq. (1) expresses the stiffness degradation of the entire model as follows:

$$f = 2\pi \sqrt{\frac{k}{m}} \quad (1)$$

where  $f$  and  $k$  are the natural vibration frequency and overall stiffness of the structure, respectively, under different working conditions;  $m$  is the mass of the structure.

From Table 5, it can be observed that

(1) With an increase in the PGA, the natural frequencies of the two stage models gradually decreased, overall stiffness degraded, and the damping ratio increased. In the first stage, after the model experienced the earthquake with a PGA of 0.07 g,  $f_x$  and  $f_y$  decreased by 6 and 5%, respectively, and the overall stiffness of the structure decreased by 11.64 and 9.83% in the X- and Y-directions, respectively. After experiencing the earthquake with a PGA of 0.10 g,  $f_x$  and  $f_y$  decreased

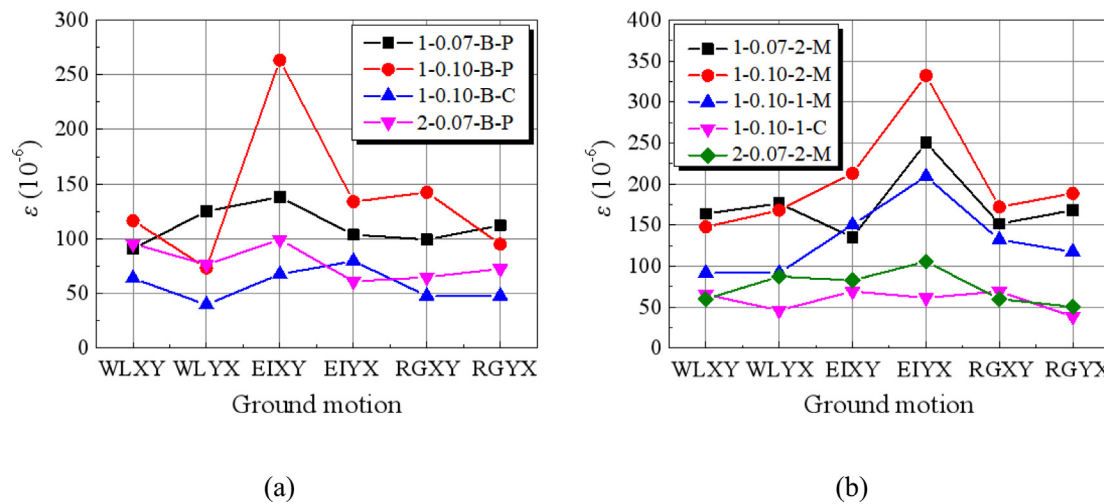


Fig. 16. Maximal strain at end column of both shear walls and general walls. (a) X-direction. (b) Y-direction.

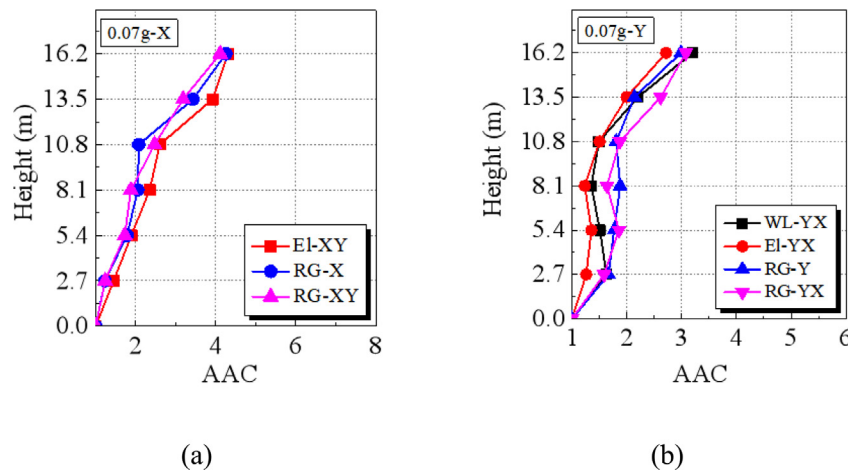


Fig. 17. Acceleration amplification factor curves of the first stage model. (a) X-direction for FOE8. (b) Y-direction for FOE8.

slightly, and the overall stiffness of the structure decreased by 1.06 and 1.76% in the X- and Y-directions, respectively, indicating that the overall stiffness of the building model changed slightly, and the structural damage was insignificant. In the second stage, during the process of loading the model from a FOE8 earthquake to a DBE8.5 earthquake, the frequency in the X-direction decreased steadily, and the wall panel exhibited significant cumulative damage. The peripheral screw connection was damaged seriously, and the skin effect was significantly weakened. In summary, after the earthquake with a PGA of 0.40 g, the  $f_x$  value of the structure did not decrease significantly, indicating that the 8 degree rare earthquake did not cause further damage to the structure.

(2) For both test models,  $f_x$  was larger than  $f_y$ , indicating that the stiffness of the structure in the X-direction was higher than that in the Y-direction, which is consistent with the actual design stiffness of the model and the experimental phenomenon that the seismic response in the X-direction was less significant than that in the Y-direction. The frequency reduction rate in the Y-direction was significantly higher than that in the X-direction because the strength of the gypsum board was lower than that of the CFB, and its screw connection was more likely to be damaged. After experiencing the earthquake with a PGA of 0.40 g, the Y-direction frequency of the second stage model was equal to the natural frequency of the first stage model, indicating that the skin effect of the gypsum board had completely failed. The natural vibration frequency of the structure in the X-direction was 2.30 Hz, which was higher than the 2.00 Hz natural vibration frequency of the model in

the first stage, indicating that although the gypsum board had been seriously damaged, the CFB was retaining the skin effect.

(3) Compared with the model in the first stage, the  $f_x$  and  $f_y$  values of the model in the second stage increased by 34 and 100%, respectively, indicating that under the condition where both the models maintained the same weight, the wall panel could resist the horizontal earthquake action together with the shear wall through the skin effect, and the overall stiffness of the building improved significantly; moreover, the skin effect in the Y-direction was higher than that in the X-direction.

## 5.2. Strain response

Furthermore, the strain response of the first stage and second stage models were analyzed. Under the seismic intensities of FOE8 and DBE7, the maximum strain value curves of typical components in axis B and axis ② are shown in Fig. 16(a) and (b), respectively. In the figure, the abscissa WLXY indicates inputting the Wolong earthquake wave, with the X- and Y-directions as the primary and secondary directions, respectively; YX indicates the reverse of the primary direction. El and RG represent the El Centro earthquake and artificial earthquake waves, respectively. In the legend "1-0.07-B-P", the four symbols consecutively represent the first stage (2 indicates the second stage), PGA of 0.07 g, B axis (1 and 2 represent axis 1 and axis 2, respectively), and steel pipe stud (M denotes the cap-shaped stud, and C denotes the C-shaped stud).

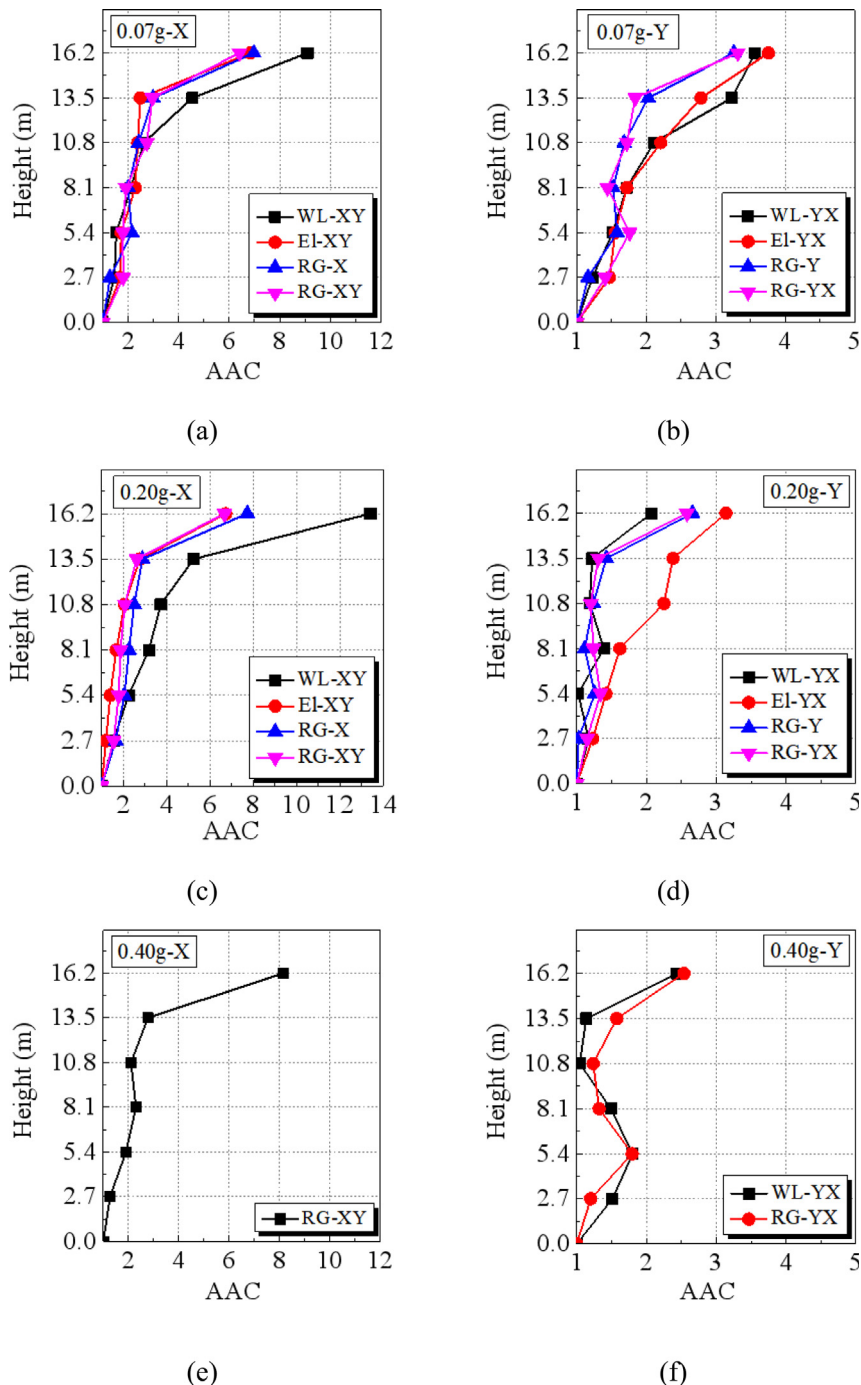


**Fig. 18.** Acceleration amplification factor curves of the second stage models. (a) X-direction for FOE8. (b) Y-direction for FOE8. (c) X-direction for DBE8. (d) Y-direction for DBE8. (e) X-direction for MCE8. (f) Y-direction for MCE8.

The strain channel was cleared at the end of each working condition; thus, the measured strain value was the members' strain increment caused by each degree earthquake. The following can be inferred based on the figure:

(1) The strains at all measuring points were the maximum under the El Centro earthquake wave, which was consistent with the experimental phenomenon that the model response was the maximum under the El Centro earthquake. Moreover, the strain response of the structural member became intense with an increase in the peak acceleration of the input seismic wave.

(2) In the first stage model, the strain of the stud of the shear wall was significantly higher than that of the ordinary wall stud,

which proves that the steel plate shear wall worked as a shear-resistant member in the multi-storey CFS-SPSWS system.

(3) Compared with the first stage model, the X- and Y-direction strains of the stud of the shear wall in the second stage model were reduced by 41% and 70%, respectively. This phenomenon indicated that the wall panels in the second stage model shared a portion of the horizontal shear force through the skin effect, resulting in a decrease in the seismic load carried by the shear wall, leading to a further decrease in the strain response.

(4) When the second stage model was loaded under the MCE8 earthquake with a PGA of 0.40 g, the maximum strain of the stud of the shear wall was below  $0.6 \times 10^{-3}$ , considerably lower than the

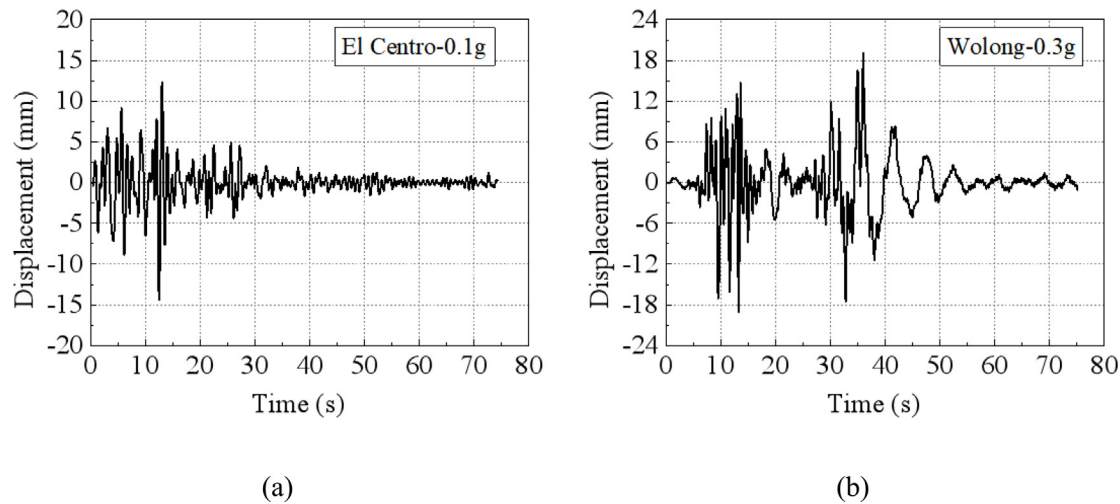


Fig. 19. Displacement time history curves of models. (a) First stage model. (b) Second stage model.

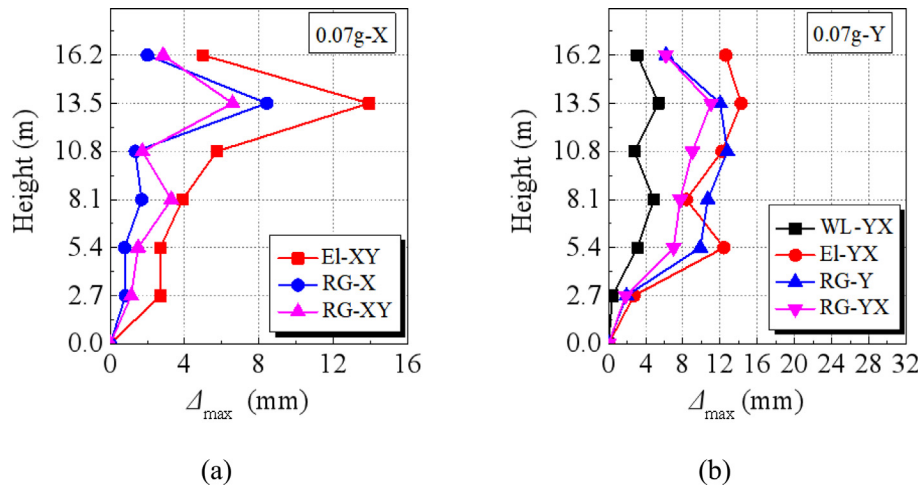


Fig. 20. Maximum displacement curves of the first model. (a) X-direction for FOE8. (b) Y-direction for FOE8.

yield strain of steel, indicating that the horizontal lateral force resistant member of multi-storey CFS-SPSWS was in an elastic working state.

### 5.3. Acceleration response

The acceleration changes under different working conditions were determined using the measured point data of the accelerometers on each floor. Fig. 17(a) and (b) show curves of the acceleration amplification factor (AAC) of the first stage model under the action of the FOE8 earthquake waves with a PGA of 0.07 g. Fig. 18 shows curves of the AAC of the second stage model under the action of the FOE8, DBE8, and MCE8 earthquakes with a PGA of 0.07 g, 0.20 g, and 0.40 g, respectively.

It can be observed from the figures that:

(1) With an increase in height, the AAC increased and reached the maximum value at the sixth storey. Under the same level of earthquake action, the AAC in the X-direction of the first stage model was larger than that in the Y-direction, indicating that the lateral stiffness in the X-direction was higher than that in the Y-direction. Due to the differences of the screw spacing and the number of sheathed panels of SW-1 shear walls in each storey, the lateral stiffnesses of the shear walls on the first storey and the second storey were the same and the biggest, and from the second storey to the sixth storey, the lateral stiffness decreased successively. Therefore, the AAC curve appeared "concave" at the location of the stories with the stiffness changes.

(2) For the second stage model, the AAC decreased with an increase in the shake table input PGA, indicating that the cumulative damage of the wall panel increased gradually, and the lateral stiffness of the common wall decreased. Furthermore, as the cumulative damage of the wall panel was serious, the skin effect was significantly weakened, and the lateral stiffness of the primary wall degraded significantly. The horizontal force of the structure was mainly carried by the steel plate shear wall. Moreover, the gradually increasing shake table input ground motion did not cause the plastic failure of the steel plate shear wall, leading to an increase in the peak AAC.

(3) Under the action of the Y-directional MCE8 earthquake with a PGA of 0.40 g, the AAC increased gradually at stories 1 and 2, decreased at floors 3 and 4, and increased again at floors 5 and 6, presenting an overall S-shaped distribution. This is likely to be related to the stiffness degeneration of the lateral force resisting members in stories 3 and 5.

### 5.4. Displacement response

Through the baseline correction and filtering of the acceleration time history curve, the absolute displacement of each measuring point was obtained using the acceleration quadratic integral method. The relative displacement of the measuring point at each storey can be obtained by subtracting the absolute displacement of the shake table from the absolute displacement of measuring points. Figs. 19(a) and (b) show the X-directional displacement time history curves for the El

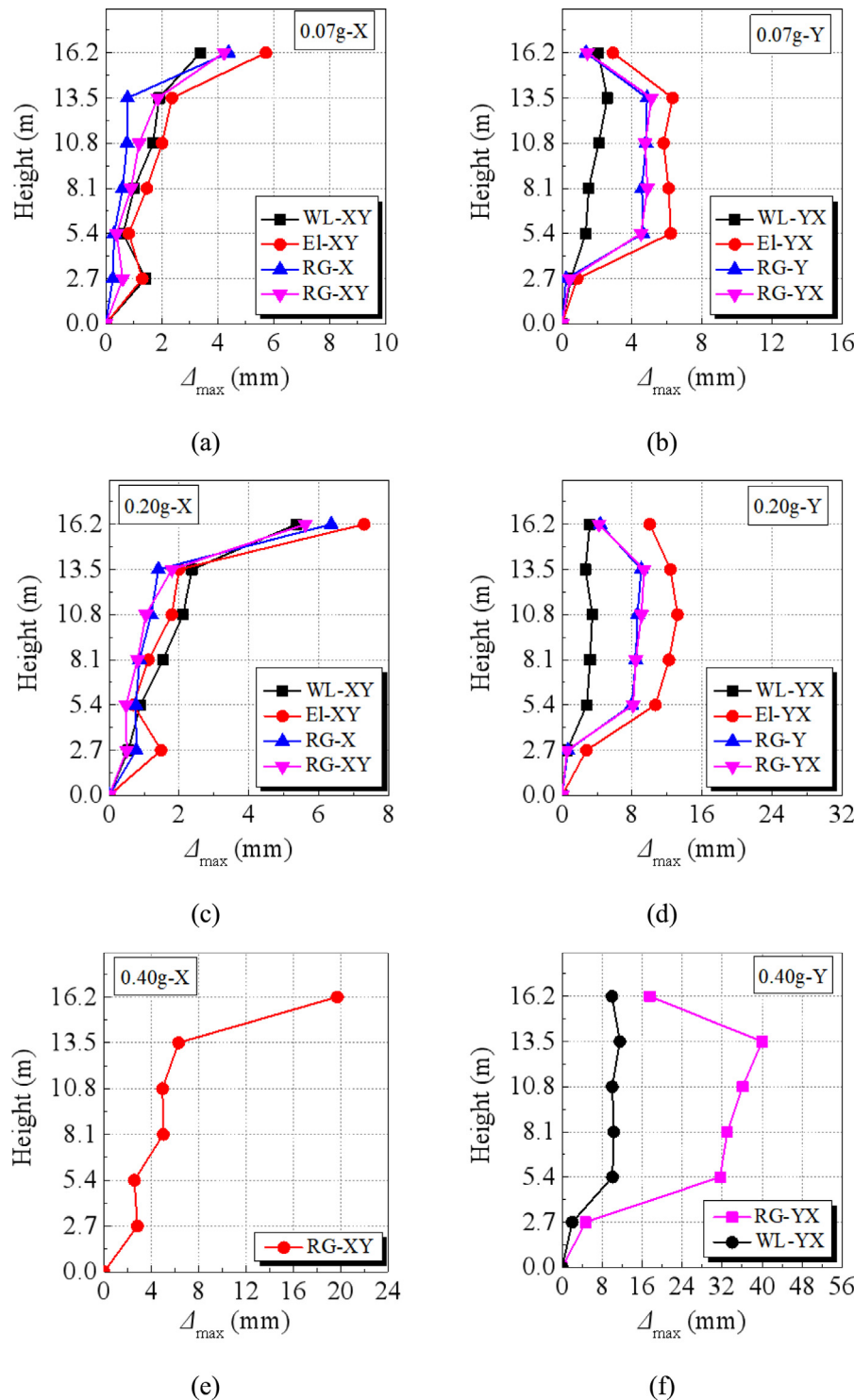


**Fig. 21.** Maximum displacement curves of the second model. (a) X-direction for FOE8. (b) Y-direction for FOE8. (c) X-direction for DBE8. (d) Y-direction for DBE8. (e) X-direction for MCE8. (f) Y-direction for MCE8.

Centro wave in the first storey of the first stage model for a PGA of 0.1 g and Wolong wave in the first storey of the second stage model with a PGA of 0.3 g, respectively.

Figs. 20(a) and (b) show the curves of the peak value of the relative displacement in the X- and Y-directions, respectively, of the first stage model under the action of the FOE8 earthquake waves. Fig. 21 shows the curves of the peak value of the relative displacement of the second stage model under the actions of the FOE8, DBE8, and MCE8 earthquakes with PGA values of 0.07 g, 0.20 g, and 0.40 g, respectively.

It can be observed from the figures that:

(1) Under the same loading conditions of the PGA of the input earthquake waves, the displacement responses of the model to the El Centro earthquake, artificial earthquake, and Wolong earthquake waves gradually decreased. The displacement of each storey of the model increased with the enhancement of the peak acceleration of the earthquake wave. (2) Compared with the first stage model, the displacement of each storey in the second stage model under the condition of the FOE8 earthquake intensity was significantly reduced. Moreover, the

maximum displacements in the X- and Y-directions decreased by 8.21 and 7.96 mm, respectively, indicating that the nonstructural components (i.e., the lightweight wall panels) could significantly improve the seismic performance of the entire structure.

The maximum inter-storey displacement angle is an important index to evaluate the seismic performance of structures. In the first stage model, the maximum inter-storey displacement angles of the structure in the X- and Y-directions were 1/302 and 1/279, respectively, under the action of the FOE8 earthquake with a PGA of 0.07 g. The above indexes satisfied the required limit of 1/250 for the elastic inter-storey displacement angle of multi-storey steel structures mentioned in the specifications [28,29]. Moreover, according to the failure phenomenon of the model in the first stage, no significant damage was observed in the structural members, and the model was in the elastic state. In the second stage of the model, the maximum inter-storey displacement angle of the structure in the X- and Y-directions were 1/748 and 1/505, respectively, under the action of the MCE8 earthquake with a PGA of 0.07 g, and the maximum inter-storey displacement angles of the structure in the X- and Y-directions were 1/201 and 1/100, respectively, under the action of the MCE8 earthquake with a PGA of 0.40 g. The above indexes satisfied the required limit for the elastic inter-storey displacement angle of 1/250 [28,29] and elastic-plastic inter-storey displacement angle of 1/50 [28] in multi-storey and high-rise steel structures. Furthermore, according to the failure characteristics of the second stage model, only cracks and screw connection failure occurred in the lightweight wall panel of the nonstructural members, and no significant plastic deformation was observed in the structural members, indicating a good ductility of the structure.

## 6. Conclusions and design suggestions

In this study, the seismic performance of the full-scale six-storey CFS-SPSWS structure was investigated through shake table tests using bidirectional ground motions as the inputs. The structural failure characteristics and effects of the nonstructural members on the seismic performance, dynamic performance, and seismic response were evaluated. The following conclusions were drawn:

(1) The failure characteristics of multi-storey CFS-SPSWS structure under the actions of earthquakes included the screw connection failure of the nonstructural members. With an increase in the ground motion intensity, a gradual failure of the wall panel was observed, the skin effect weakened, and the shear force on the steel plate shear walls increased gradually. It should be noted that Shi et al. [30] have provided an excellent method to simulate the screw connections in CFS walls, and this method could also be used to model the screw connections in the CFS-SPSWS structure.

(2) With an increase in the PGA, the natural frequency of the first stage model decreased slightly, indicating that the structure was always in the elastic stage without any significant damage. In the second stage, the wall panel screw connection of the model was gradually damaged to failure, and the natural vibration frequency and structural stiffness of the structure decreased.

(3) The light wall panel of the nonstructural members increased the natural vibration frequency and acceleration response of the structure and reduced the strain response of the structural members, floor deformation, and inter-storey displacement angle of the structure. This shows that the skin effect of the wall panel and steel plate shear wall together resisted the horizontal shear, improved the seismic performance of the overall structure, and absorbed and dissipated the seismic energy in the elastic-plastic stage of the wall panel. This effectively protected the structural members and the overall structure.

(4) After several repeated seismic tests, the six-storey full-scale CFS-SPSWS model exhibited no collapse risk, and there was no significant plastic damage to the structural members. The maximum inter-storey displacement angle under the action of the FOE8 and MCE8 earthquakes satisfied the specification requirements. This shows that the

multi-storey CFS-SPSWS adopting CFS -clamped steel plate shear walls and CFS-steel plate sheathed shear walls as horizontal lateral force resisting components could achieve good deformation capacity and seismic performance.

Based on the design process and experimental results of the multi-storey CFS-SPSWS, the following design recommendations were proposed:

- (1) **Architectural layout.** The building plane of the multi-storey CFS-SPSWS shall be simple, regular and symmetrical, so that the wind load and seismic load are evenly distributed on the plane. The biaxial symmetrical plane can effectively avoid the torsional effect of the structure due to horizontal load. The elevation of the multi-storey CFS-SPSWS should choose simple shapes with rectangular, trapezoidal and other vertical dimensions changing linearly along the height, to better carry out the horizontal seismic and wind resistance design of the structure.
- (2) **Arrangement of shear walls.** To establish a clear horizontal lateral force resisting system, the CFS shear walls shall be evenly arranged in the two principal axes direction of the structural plane and vertical direction of the multi-storey CFS-SPSWS. To ensure that the horizontal force of the roof and floor can be effectively transmitted to the foundation, a reliable connection method should be adopted to make the shear walls of each floor continuously connected, and the upper and lower ends of the shear walls should be extended to the roof and foundation respectively.
- (3) The horizontal wind load and seismic action shall be borne by the shear walls, and the contribution of the skin effect of the light weight wall panels to the lateral resistance of the structure shall be not considered. The vertical load shall be borne by columns. Overturning moments will occur to the shear wall under horizontal earthquake action, and the axial force generated by the overturning moment is borne by the end stud of the wall. Therefore, when calculating the strength and stability of end columns at the shear walls, the axial force caused by the overturning moment shall be considered.

## CRediT authorship contribution statement

**Xuhong Zhou:** Supervision, Methodology, Funding acquisition, Conceptualization. **Xinmei Yao:** Writing – review & editing, Writing – original draft, Methodology, Investigation, Funding acquisition. **Lei Xu:** Writing – review & editing, Methodology, Conceptualization. **Yu Shi:** Writing – review & editing, Resources, Methodology, Investigation. **Ke Ke:** Software, Resources. **Liping Liu:** Software, Methodology, Investigation.

## Declaration of competing interest

The authors declare that they have no known competing financial interests or personal relationships that could have appeared to influence the work reported in this paper.

## Data availability

The authors do not have permission to share data.

## Acknowledgments

The authors wish to acknowledge the support of the Natural Science Foundation of China (No. 51890902), Academician of Chongqing Leads the Special Project of Guiding Scientific and Technological Innovation (No. csc2021yszx-jcyj0003), and the Natural Science Foundation Research Project of Shaanxi Province (No. 2022JQ-570). Any opinions, findings, and conclusions or recommendations expressed in this paper are those of the authors and do not necessarily reflect the views of the sponsors.

## References

- [1] K.D. Peterman, M.J.J. Stehman, R.L. Madsen, et al., Experimental seismic response of a full-scale cold-formed steel-framed building. I: System-level response, *J. Struct. Eng.* 142 (12) (2016) 04016127.
- [2] K.D. Peterman, M.J.J. Stehman, R.L. Madsen, et al., Experimental seismic response of a full-scale cold-formed steel-framed building. II: Subsystem-level response, *J. Struct. Eng.* 142 (12) (2016) 04016128.
- [3] Y.Q. Li, Z.Y. Shen, X.Y. Yao, et al., Experimental investigation and design method research on low-rise cold-formed thin-walled steel framing buildings, *J. Struct. Eng.* 139 (5) (2013) 818–836.
- [4] Z.G. Huang, M.Z. Su, B.K. He, et al., Shaking table test on seismic behaviors of three-story cold-formed thin-walled steel residential buildings, *China Civ. Eng.* J. 44 (2) (2011) 72–81 (in Chinese).
- [5] L. Fiorino, V. Macillo, R. Landolfo, Shake table tests of a full-scale two-story sheathing-braced cold-formed steel building, *Eng. Struct.* 151 (2017) 633–647.
- [6] M.T. Terracciano, B. Bucciero, T. Pali, et al., Shake table tests of structures with CFS strap-braced stud walls, *Key Eng. Mater.* 763 (2018) 432–439.
- [7] L. Fiorino, B. Bucciero, R. Landolfo, Shake table tests of three storey cold-formed steel structures with strap-braced walls, *Bull. Earthq. Eng.* 17 (7) (2019) 4217–4245.
- [8] AISI, North American Standard for Seismic Design of Cold Formed Steel Structural Systems, AISI-S400-15, American Iron and Steel Institute, Cleveland, North American, 2015.
- [9] Y. Guan, X.H. Zhou, X.M. Yao, et al., Seismic performance of prefabricated sheathed cold-formed thin-walled steel buildings: Shake table test and numerical analyses, *J. Construct. Steel Res.* 167 (2019) 105837.
- [10] S. Selvaraj, M. Madhavan, Criteria for selection of sheathing boards in cold-formed steel wall panels subjected to bending: Construction applications and performance-based evaluation, *Pract. Period. Struct. Des. Constr.* 26 (1) (2021) 04020044.
- [11] S. Selvaraj, M. Madhavan, Influence of sheathing-fastener connection stiffness on the design strength of cold-formed steel wall panels, *J. Struct. Eng.* 146 (10) (2020) 04020202.
- [12] S. Selvaraj, M. Madhavan, Investigation on sheathing-fastener connection failures in cold-formed steel wall panels, *Structures* 20 (2019) 176–188.
- [13] S. Selvaraj, M. Madhavan, H.H. Lau, Sheathing-fastener connection strength-based design method for sheathed CFS point-symmetric wall frame studs, *Structures* 33 (2021) 1473–1494.
- [14] S. Selvaraj, M. Madhavan, Direct stiffness-strength method design for sheathed cold-formed steel structural members-recommendations for the AISI S100, *Thin-Walled Struct.* 162 (2021) 107282.
- [15] X. Wang, E. Pantoli, T.C. Hutchinson, et al., Seismic performance of cold-formed steel wall systems in a full-scale building, *J. Struct. Eng.* 141 (10) (2015) 04015014.
- [16] T.C. Hutchinson, X. Wang, G. Hegemier, et al., Earthquake and postearthquake fire testing of a midrise cold-formed steel-framed building. I: Building response and physical damage, *J. Struct. Eng.* 147 (9) (2021) 04021125.
- [17] X. Wang, T.C. Hutchinson, Earthquake and postearthquake fire testing of a midrise cold-formed steel-framed building. II: Shear wall behavior and design implications, *J. Struct. Eng.* 147 (9) (2021) 04021126.
- [18] J.H. Ye, L.Q. Jiang, Simplified analytical model and shaking table test validation for seismic analysis of mid-rise cold-formed steel composite shear wall building, *Sustainability* 10 (9) (2018) 3188.
- [19] L.Q. Jiang, X.S. Zhang, J.H. Ye, et al., Seismic behavior and damage assessment of mid-rise cold-formed steel-framed buildings with normal and reinforced beam-column joints, *Arch. Civ. Mech. Eng.* 21 (2021) 125.
- [20] J. Qiu, Q. Zhao, Z. Wang, et al., Lateral behavior of trapezoidally corrugated wall plates in steel plate shear walls, part 1: Elastic buckling, *Thin-Walled Struct.* 174 (2022) 109104.
- [21] J. Qiu, Q. Zhao, C. Yu, et al., Lateral behavior of trapezoidally corrugated wall plates in steel plate shear walls, part 2: Shear strength and post-peak behavior, *Thin-Walled Struct.* 174 (2022) 109103.
- [22] W. Zhang, C. Yu, M. Mahdavian, Seismic performance of cold-formed steel shear walls using corrugated sheathing with slits, *J. Struct. Eng.* 145 (4) (2019) 04019014.
- [23] W. Zhang, M. Mahdavian, C. Yu, Different slit configuration in corrugated sheathing of cold-formed steel shear wall, *J. Construct. Steel Res.* 150 (2018) 430–441.
- [24] C. Yu, Y. Tian, W. Yan, et al., Novel energy dissipation bracing designed for corrugated sheet-sheathed cold-formed steel shear wall, *J. Struct. Eng.* 147 (11) (2021) 04021171.
- [25] Y. Shi, Z.Q. Luo, Y.P. Xu, et al., Experimental study on the seismic behavior of high-performance cold-formed steel plate shear walls, *Eng. Struct.* 251 (2022) 113552.
- [26] L. Xu, S.G. Zhang, C. Yu, Determination of equivalent rigidities of cold-formed steel floor systems for vibration analysis, part II: Evaluation of the fundamental frequency, *Thin-Walled Struct.* 132 (2018) 1–15.
- [27] GAQSIQ and SAC, Load Code for the Design of Building Structures, GB 50009-2012, General Administration of Quality Supervision, Inspection and Quarantine of P.R. China, Standardization Administration of P.R. China, Beijing, China, 2012 (in Chinese).
- [28] GAQSIQ and SAC, Code for Seismic Design of Buildings, GB 50011-2010, General Administration of Quality Supervision, Inspection and Quarantine of P.R. China, Standardization Administration of P.R. China, Beijing, China, 2010 (in Chinese).
- [29] MHURD, Technical Standard for Cold-Formed Thin-Walled Steel Multi-Storey Residential Buildings, JGJ/T 421-2018, Ministry of Housing and Urban-Rural Development, Beijing, China, 2018 (in Chinese).
- [30] Y. Shi, X.W. Ran, W. Xiao, et al., Experimental and numerical study of the seismic behavior of cold-formed steel walls with diagonal braces, *Thin-Walled Struct.* 159 (2021) 107318.